International Journal of Thermophysics, Vol. 22, No. 3, 2001

Reference Values of the Dielectric Constant of Natural Gas Components Determined with a Cross Capacitor

M. R. Moldover[1, 2] and T. J. Buckley[1]

Received November 1, 2000

A novel toroidal cross capacitor was used to measure accurately the dielectric polarizability $\varepsilon(p)$ (i.e., the dielectric constant as a function of the pressure) of helium, argon, nitrogen, methane, and carbon dioxide at $T = 50°C$. The data extend up to 7 MPa (5 MPa for CO_2) and may be useful for calibrating on-line, capacitance-based systems that are designed to measure the heating value of natural gas. The uncertainties of ε and p are 4×10^{-6} and $(3.0 \times 10^{-5} p + 84$ Pa), respectively. The properties of helium that had been calculated *ab initio* from quantum mechanics were used to verify that the cross capacitor deformed in a predictable manner under hydrostatic (gas) pressure. Thus, a common cause of systematic errors in measuring the dielectric constant of gases was avoided. For helium, the rms deviation of $\varepsilon(p)$ from the calculations was only 2.7×10^{-7}. This suggests that the estimated uncertainty is very conservative.

KEY WORDS: argon; carbon dioxide; cross capacitor; dielectric constant; dielectric polarizability; helium; methane; molar polarizability; natural gas; nitrogen; reference data.

1. INTRODUCTION

Accurate measurements of the dielectric polarizability [i.e., the dielectric constant $\varepsilon(p, T)$] are an important part of a program to determine the heating value of natural gas in pipelines from on-line measurements [1]. The planned on-line measurements will determine (p, T) from the resonance frequency of a gas-filled, reentrant cavity used as the frequency-determining element of an electromagnetic oscillator. Here, we provide values of $\varepsilon(p)$ for helium, argon, nitrogen, methane, and carbon dioxide at $T = 50°C$ and

[1] Process Measurements Division, National Institute of Standards and Technology, 100 Bureau Drive, Stop 8360, Gaithersburg, Maryland 20899-8360, U.S.A.

[2] To whom correspondence should be addressed. E-mail: michael.moldover@nist.gov

0195-928X/01/0500-0859$19.50/0

at pressures p up to 7 MPa (5 MPa for CO_2). We believe that the present data are the most accurate data available for these conditions. Thus, they can be used to calibrate reentrant cavity oscillators and to test them for systematic errors.

One of the present authors helped develop reentrant cavities for measuring the $\varepsilon(p, T)$ of gases and also of weakly conducting liquids such as water [2, 3]. During the development process, it became clear that reentrant cavities should be calibrated and tested to account for three effects: (1) the deformation of the cavity under the pressure of the test fluid, (2) the presence of dielectric layers on the metal surfaces of the cavity, (e.g., a permanent oxide, a deposited oil film, or an adsorbed layer of gas), and (3) the frequency dependence of the circuit model for the reentrant cavity. (Frequency-dependent quantities include the electromagnetic penetration depth, the coupling to the external circuitry, and the magnetic susceptibility of some metals.) In the present work, the values of $\varepsilon(p, T)$ are not subject to the errors from these three effects. The first effect was minimized by design, then calculated, and, finally, confirmed by measurement. The second and third effects are very small.

The present data were obtained using a toroidal cross capacitor. In its simplest form, a cross capacitor is composed of four conducting cylindrical electrodes separated by small, insulating gaps and arranged to form a closed surface [4, 5]. The cross capacitance C_x is the average (with weight w [6]) of the two capacitances measured between opposite pairs of electrodes. In the notation of Fig. 1,

$$C_x \equiv wC_{TB} + (1 - w)\, C_{IO} \tag{1}$$

An appropriate choice of w compensates for many possible problems. For example, if a thin oil layer were deposited on the bottom electrode, it would tend to increase C_{TB} and decrease C_{IO}. If the cross capacitor were suitably designed, a uniform dielectric layer of thickness t would change C_x in proportion to $(t/h)^2$, where h is the distance between opposite pairs of electrodes. In contrast, the same dielectric layer would change the capacitance of a reentrant cavity in proportion to (t/h). For this work, the sensitivity to dielectric layers is even smaller because h is much larger than the gap of a typical reentrant cavity (9.5 mm *versus* 1 mm).

In Section 2, we describe the cross capacitor, emphasizing the calculation of its deformation under hydrostatic pressure. Section 3 describes the instruments, materials, and procedures that were used to make the measurements and the contributions of each to the uncertainty of the final results. We note that the capacitances C_{TB} and C_{IO} were measured with a bridge operating at the low frequency of 1 kHz; thus, it was not necessary

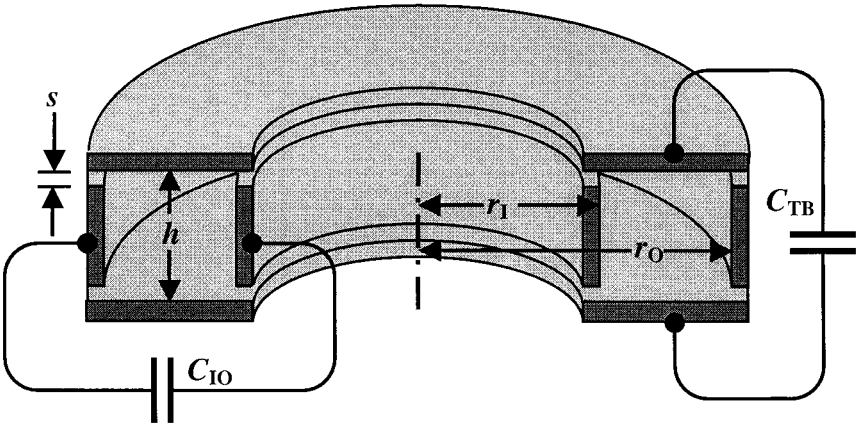

Fig. 1. Schematic cross section of the toroidal cross capacitor. The washer-shaped top and bottom electrodes comprise the capacitor $C_{TB} \approx 0.72$ pF. The tube-shaped inner and outer electrodes comprise the capacitor $C_{IO} \approx 0.52$ pF. The grounded shield that surrounds these electrodes is shown in Fig. 2. The dimensions were $s \approx 0.15$ mm, $r_I \approx 45$ mm, $r_O \approx 55$ mm, and $h \approx 9.5$ mm.

to make assumptions about the frequency dependence of the electromagnetic penetration depth. Section 4 discusses tests of the performance of instruments and the cross capacitor that we made while the capacitor was under vacuum and under pressure from helium. These tests used some properties of helium calculated *ab initio* from quantum mechanics as a standard. The tests demonstrated that the pressure dependence of C_x was consistent with the model of the cross capacitor. We urge all who make accurate measurements of $\varepsilon(p, T)$ to conduct similar tests.

In Section 5, we tabulate the reference data for $\varepsilon(p)$ for each gas. In Section 6, we compare the present results with results from the literature. For methane, this is done graphically. For argon, nitrogen, and CO_2, the comparison is made using the dielectric virial coefficients A_ε and b that appear in the expansion of the molar polarizability $\wp$ as a function of the molar density ρ:

$$\wp(\rho, T) = \left(\frac{\varepsilon - 1}{\varepsilon + 2}\right)\frac{1}{\rho} = A_\varepsilon(1 + b\rho + c\rho^2 + \cdots) \tag{2}$$

In general, the coefficients A_ε, b, c,... are temperature dependent. The temperature dependence of A_ε is small; for the monatomic gases, it is too small to measure. (Some authors define the "dielectric virial coefficients" by $B_\varepsilon \equiv A_\varepsilon b$, $C_\varepsilon \equiv A_\varepsilon c$, etc. With the present definition, it is easy to compare the dielectric virial coefficients with the density virial coefficients.) We

believe that our values of A_ε are more accurate than previously published values. Our values of b are consistent with many published values; however, they may be less accurate than the published values that were obtained using expansion techniques. The reader is warned that if Eq. (2) is used with parameters from Table II and an equation of state to calculate $\varepsilon(p, T)$, the results will be less accurate than our $\varepsilon(p, T)$ data, unless the equation of state is the same as that used here to determine A_ε, b, and c.

2. CROSS CAPACITORS

In a recent publication, we described two toroidal cross capacitors, designated C_1 and C_2,that were designed for measuring the dielectric constant of gases [7]. There, we discussed details of their construction, tests of their performance, and lessons learned. In the present work, we used capacitor C_1 without modification. However, we replaced the pressure vessel with a new one that could be used up to 10 MPa. Here, we limit the discussion to a few general remarks and a discussion of the deformation of the cross capacitor under hydrostatic pressure.

2.1. General Remarks

Since the 1960s, national metrology institutes have used large (of the order of 1 m long), evacuated cross capacitors as impedance standards to realize the ohm. Subsequently, Shields [8] used a toroidal cross capacitor as a standard for the absolute measurement of the loss angle of conventional capacitors and also to verify that cross capacitors are insensitive to dielectric films on their electrodes. Despite this long history, we have not found earlier measurements of the dielectric constants of fluids that used cross capacitors. There are several reasons for this. First, cross capacitors are more complicated to manufacture than other capacitors, because they must have at least four electrodes that are insulated from one another. Second, an array of very well-shielded switches is required to connect each electrode pair to a bridge while its capacitance is being measured and then to ground while the capacitance of the other pair is being measured. Third, cross capacitors have very low capacitances. In vacuum, the capacitance is $C_x = (\varepsilon_0 \ln 2)/\pi = 1.953\,549\ldots$ pF per meter of length, where the electric constant $\varepsilon_0 = 8.854\,187\,817\ldots \times 10^{-12}\ \mathrm{F \cdot m^{-1}}$. Finally, two measurements of capacitance are required to determine each value of C_x. Thus, each measurement of C_x takes more time.

The cross capacitor used in this work is shown in Figs. 1 and 2. It was composed of four coaxial electrodes, each having a rectangular cross section. The four electrodes were arranged to enclose a toroidal volume with a nearly

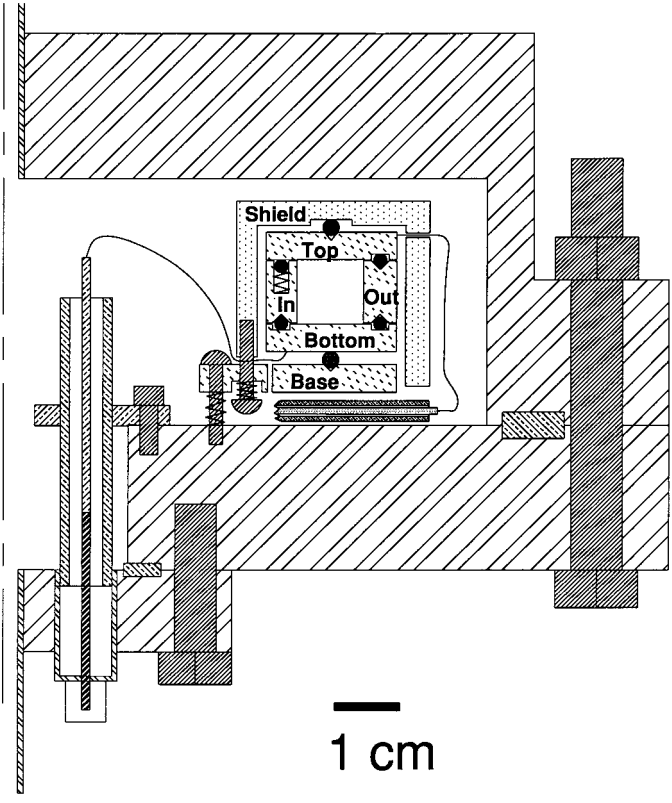

Fig. 2. Scale drawing of a section of the cross capacitor within its pressure vessel. Coaxial cables are sketched.

square cross section. The two electrodes designated "top" and "bottom" were shaped like washers. The two electrodes designated "inner" and "outer" were tube-shaped. All four electrodes were made from superinvar, an alloy chosen for its very small coefficient of thermal expansion. Sapphire balls were used to insulate the electrodes from each other and to support the bottom electrode on a grounded, superinvar base. The electrodes were surrounded by a grounded aluminum shield that was separated from the top electrode by sapphire balls. The entire electrode structure was enclosed by the pressure vessel shown in Fig. 2.

The sapphire balls and superinvar electrodes were assembled into a kinematically stable structure. Three radial "V" grooves were electrodischarge machined into the top and bottom electrodes, and three mating cavities were electrodischarge machined into the inner and outer electrodes. The electrodes and balls were pressed together by springs.

Theory [9] has provided several useful results for toroidal cross capacitors with nearly square cross sections, i.e., cross sections with height $h \approx \text{width} = (r_O - r_I)$. These results include

$$C_x = 2 \ln 2 \, r\varepsilon_0 \varepsilon f(h/r, s/h)$$
$$f(h/r, s/h) = 1 - 0.04042(h/r)^2 - 0.0017(s/h)^2 + \cdots \tag{3}$$

For our cross capacitor, the average radius of the tori is $r = (r_O + r_I)/2 \approx 50$ mm. The cross section of our capacitor deviated from a square. (In vacuum, $C_{TB} \approx 0.72$ pF and $C_{IO} \approx 0.52$ pF.) A measure of the deviation is $\delta \equiv 1 - (\text{height})/(\text{width}) \approx 0.05$. We used the theoretical result,

$$C_x = 2 \ln 2 \, r\varepsilon_0 \varepsilon (1 + 3.454\delta^2 + \cdots) \tag{4}$$

to choose the weight $w = 0.4476$ in Eq. (1) such that $(\partial C_x/\partial \delta) = 0$. With this choice, small movements of the top or bottom electrodes with respect to the inner and outer electrodes changed C_x only in the second order. For example, if the top electrode in Fig. 1 is raised, thereby increasing the gap s by Δs, C_{TB} will decrease and C_{IO} will increase. The ratio $C_{TB}/C_{IO} \approx 1.38$ will decrease; however, the fractional change in C_x will be much smaller, of the order of $s \times \Delta s/h^2$. In Section 4.2, we provide evidence that such movement did occur when the pressure was changed and that the movement did not affect C_x within the resolution of the measurements.

With the asymmetric weighting of C_{TB} and C_{IO}, the cross capacitance depends, in the first order, only on the average radius $r = (r_O + r_I)/2$ of the tori. This average is determined solely by the inner radius of the outer electrode and the outer radius of the inner electrode. Each electrode was made from a superinvar plate, and each was subject to only small external forces from springs, gravity, and buoyancy. Thus, we expected that the pressure and temperature dependences of r and C_x would be those of superinvar alone.

An effort was made to isolate the cross capacitor from the relatively large, pressure-dependent deformation of the pressure vessel that enclosed it. The base of the cross capacitor was supported by three helical springs. Each spring was wound around a smooth shaft to constrain it. The end of each shaft was threaded and screwed into a blind, threaded hole in the pressure vessel. The clearance holes in the base plate were oversized to avoid stressing the plate.

2.2. Predicted Response to Pressure

If the cross capacitor were completely uncoupled from the pressure vessel, it would still deform when gas pressure was applied. This deformation

was calculated from the geometry of the cross capacitor and the elastic properties of the materials used to construct it. The calculation was confirmed by an experimental test: the pressure vessel was filled with compressed helium at 50°C, $\varepsilon(p)$ was measured, and the results were compared with $\varepsilon(p)$ calculated using *ab initio* results from quantum mechanics for the dominant terms. (See Section 4.)

Because C_x depends so weakly on the insulating gaps [Eq. (3)], the isothermal volumetric compressibility $k_T \equiv -(\partial V/\partial p)_T/V$ of the superinvar is the material property that determines the pressure dependence of C_x. To measure k_T, three small samples were cut out of the superinvar plates when they were received from the manufacturer. A. Migliori (Los Alamos National Laboratory) used the well-established technique [10] of resonant ultrasound spectroscopy (RUS) to measure the adiabatic compressibility of these samples at ambient temperature. The RUS result was $k_S^{-1} = (1.06 \pm 0.04) \times 10^{11}$ Pa, where the standard uncertainty was calculated from the different results for the three samples. From published thermodynamic data for superinvar, one can show that the difference between the adiabatic compressibility k_S and the isothermal compressibility k_T is negligible. Also negligible is the change in k_T from 20°C, where it was measured, to 50°C, where it was used. The superinvar electrodes were heat treated before the capacitor was assembled. After heat treatment, three additional samples were cut out of the electrodes; however, the ultrasonic resonances in these post-treatment samples had quality factors that were too low to use RUS.

Under the hydrostatic pressure p, the deformation of the superinvar was small and, by assumption, isotropic. Then all linear dimensions and, thus, C_x decreased by the factor $k_T p/3$. To account for this, the working equation for ε is

$$\varepsilon(p) = \frac{C_x(p)}{C_x(0)}(1 + k_T p/3) \tag{5}$$

To estimate the importance of k_T, we combine Eqs. (2) and (5) and eliminate the density using the virial equation of state,

$$p = \rho RT(1 + B\rho + C\rho^2 + D\rho^3 + \cdots) \tag{6}$$

where $R = (8.314\,472 \pm 0.000\,015)\ \mathrm{J \cdot mol^{-1} \cdot K^{-1}}$ is the molar gas constant, and B, C, and D are the density virial coefficients. This leads to the expression

$$C_x(p)/C_x(0) = [1 + 3A_\varepsilon \rho_0(1 + \beta\rho_0 + \gamma\rho_0^2 + \delta\rho_0^3 + \cdots)]/(1 + k_T RT\rho_0/3) \tag{7}$$

Here, we have used the definitions

$$\begin{aligned} \rho_0 &= p/(RT) \\ \beta &= -B + b + A_\varepsilon \\ \gamma &= -C + 2B^2 - 2A_\varepsilon B - 2Bb + A_\varepsilon^2 + 2A_\varepsilon b + c \\ \delta &= -D + 5BC - 5B^3 + f(A_\varepsilon, b, c, d) \end{aligned} \tag{8}$$

When the right-hand side of Eq. (7) is expanded, the coefficient of ρ_0 is $3(A_\varepsilon - k_T RT/9)$. Thus, the term $k_T RT/9 = (2.81 \pm 0.11) \times 10^{-3}\ \mathrm{cm}^3 \cdot \mathrm{mol}^{-1}$ behaves as a correction to A_ε. For methane ($A_\varepsilon \approx 6.55\ \mathrm{cm}^3 \cdot \mathrm{mol}^{-1}$), this correction for the compressibility of the superinvar is equivalent to 0.043% of A_ε and its uncertainty is equivalent to 0.0016% of A_ε. For helium ($A_\varepsilon \approx 0.517\ \mathrm{cm}^3 \cdot \mathrm{mol}^{-1}$), this correction is 13 times more important.

3. INSTRUMENTS AND MATERIALS

Here, we consider how the measurements of pressure, temperature, and capacitance contribute to the uncertainty of the results. The effects of possible impurities in the test gases are also considered.

3.1. Pressure

During the dielectric constant measurements, the pressure of the gas surrounding the capacitor was set by a DH Instruments Model PPCK pressure controller/calibrator. Two DH Instruments[3] Model RPM-1 pressure sensors were used to monitor the pressure in the manifold. One of the sensors was better behaved, and its readings were used to prepare Table I. Both pressure sensors were fully calibrated at the beginning and near the end of the 2-month-long interval used to obtain the data. Partial calibrations were conducted twice during the interval and at the end of the interval.

The standard for the calibration was a DH Instruments Model PG7001 piston gage used in the absolute pressure mode with piston-cylinder set No. 360. The uncertainty of the piston gage measurements was dominated by the 27-ppm uncertainty of the effective area of the gage

[3] To describe materials and experimental procedures adequately, it is occasionally necessary to identify commercial products by manufacturer's name or label. In no instance does such identification imply endorsement by the National Institute of Standards and Technology, nor does it imply that the particular product or equipment is necessarily the best available for the purpose.

Table I. Values of the Dielectric Constant at 50°C[a]

Methane		Nitrogen		Carbon dioxide		Argon		Helium	
p (kPa)	$100(\varepsilon-1)$	p (kPa)	$100(\varepsilon-1)$	p (kPa)	$100(\varepsilon-1)$	p (kPa)	$100(\varepsilon-1)$	p (kPa)	$100(\varepsilon-1)$
0.02	0.00000	0.01	0.00000	0.00	0.00000	0.00	0.00000	0.02	0.00000
1039.25	0.77204	1022.02	0.50161	754.96	0.64061	914.46	0.42505	974.98	0.05609
2022.28	1.52527	2004.01	0.98491	1631.94	1.44442	1924.62	0.89953	1964.64	0.11256
3025.54	2.31724	2997.80	1.47488	2336.40	2.14471	2920.62	1.37209	2962.57	0.16900
3997.67	3.10686	3996.65	1.96755	3041.22	2.90353	3944.49	1.86245	3925.70	0.22310
4969.91	3.91806	4996.93	2.46063	3752.98	3.74002	4960.10	2.35308	4933.69	0.27926
5995.32	4.79599	5983.88	2.94623	4453.82	4.64760	5976.10	2.84755	5960.13	0.33593
6879.37	5.57100	6989.45	3.43952	4973.56	5.38631	6992.69	3.34559	6992.78	0.39246
6193.61	4.96839	5999.08	2.95366	4438.27	4.62651	5984.44	2.85162	6010.99	0.33871
5983.51	4.78585	5008.68	2.46638	3764.73	3.75460	4966.81	2.35629	4976.76	0.28163
5004.28	3.94717	4005.78	1.97203	3052.67	2.91640	3952.40	1.86621	3957.47	0.22485
4000.52	3.10925	3003.43	1.47763	2335.28	2.14360	2933.32	1.37812	2939.42	0.16768
2999.91	2.29676	1999.92	0.98290	1626.95	1.43965	1916.61	0.89573	1922.31	0.11014
2001.61	1.50927	991.79	0.48674	920.32	0.78698	899.60	0.41811	895.48	0.05151
997.58	0.74061	0.00	−0.00004	0.00	0.00001			−0.02	0.00000
−0.02	0.00001								

[a] The fractional uncertainty of ε is 4×10^{-6}, based on the specification of the capacitance bridge. We believe that this uncertainty is conservative because the rms deviation of the helium data from the calculations is 2.7×10^{-7}.

(1 ppm = 1 part in 10^6) The uncertainties of the masses, the local acceleration of gravity, and the pressure head were much smaller. The manufacturer's specification for the total uncertainty was "30 ppm + 4 Pa."

The sensors were calibrated in a series of 1-MPa steps, first increasing from 1 to 7 MPa and then decreasing back to 1 MPa. Approximately 15 min was allowed for equilibration between steps. A linear regression was used to represent the calibration data. Between the calibrations, the scale factor of the better sensor changed by 7 ppm or less and its zero-pressure intercept changed by 130 Pa or less. These changes were correlated such that the maximum change between calibrations was 55 Pa at 7 MPa. The deviations from the linear regressions were systematic; the sensor readings were lower than those for the standard when the pressure was increased, and they were higher than those for the standard when the pressure was decreased. Consistent with this hysteresis, the pressure sensor had a positive reading under vacuum at the start of each measurement cycle and a negative reading under vacuum at the end of each cycle. The largest deviation from the calibration function was 102 Pa, and the root mean square (rms) deviation was 64 Pa. This hysteresis propagated into the data for $\varepsilon(p, T)$, where its size was approximately the product $(64\ \text{Pa}) \times (\partial\varepsilon/\partial p)_T$, which ranges from 3.6×10^{-8} for helium to 7×10^{-7} for carbon dioxide.

In summary, we estimate that the uncertainty of the pressure measurements was the quadrature sum of three terms: $30 \times 10^{-6} p$ from the uncertainty of the standard, 55 Pa from changes of the calibration function between calibrations, and 64 Pa from the rms deviations of readings from the calibration functions. We represent this uncertainty as $(3 \times 10^{-5} p + 84\ \text{Pa})$.

3.2. Temperature

The cross capacitor was enclosed in a pressure vessel that was immersed in a stirred oil bath. Whenever gas was admitted into or removed from the pressure vessel, we waited 3 to 7 h (depending upon the gas being studied) for the capacitor temperature to return to the bath temperature.

The capacitor temperature was inferred from two temperature probes, one immersed in the bath and the other between the flanges of the pressure vessel. Both probes were calibrated in the bath using a long-stemmed standard platinum resistance thermometer that had been calibrated on ITS-90. The largest uncertainty in the temperature measurements resulted from temperature gradients within the bath. The gradients were measured by moving a thermistor to 14 locations in the bath surrounding the pressure vessel. In one arrangement of the bath, the standard deviation of

the thermistor temperatures was 3.9 mK (corresponding to $12 \times 10^{-6} T$); in another arrangement it was 2.5 mK. In either case, the relative uncertainty of the temperature was much smaller than the relative uncertainty of the pressure. Therefore, the uncertainties of the temperature made a negligible contribution to the uncertainty of $\varepsilon(p, T)$.

All of the data were taken when the bath was within 20 mK of 50.00°C. In Table I, the results are reported at exactly 50°C. The derivative $(\partial p/\partial T)_\rho$ used to adjust the measured pressures to the tabulated pressures was taken from the recommended equations of state in NIST Standard Reference Database 12, Version 5.0 [11].

3.3. Capacitance

All capacitance measurements were made using an automated bridge (Model AH-2500A, Option E) manufactured by Andeen-Hagerling Inc. The manufacturer provided the following specifications: "accuracy of 3 ppm," "true resolution of 0.5 aF and 0.07 ppm," and "stability better than 0.5 ppm/year." The bridge was frequently self-calibrated according to the manufacturer's instructions.

Coaxial cables with grounded shields led from the bridge to an array of coaxial relays (Model 7102; Matrix Systems, Inc.). During each capacitance measurement, all of the conductors were grounded via the relays except the two electrodes that were connected to the bridge. The capacitance bridge also measured the conductance associated with the capacitor and its cables. Typically, the conductance was equivalent to a leakage resistance of $10^{12}\Omega$ in the coaxial cables.

In the present work, $\varepsilon(p, T)$ was computed from capacitance ratios $C_x(p)/C_x(0)$, where $C_x(p)$ was the cross capacitance at pressure p and $C_x(0)$ was the cross capacitance under vacuum. Because of the time required for thermal equilibration, a measurement cycle took a few days. Thus, the stability of the bridge during these intervals was important. The cross capacitance was computed from the weighted average of C_{TB} and C_{IO}. These capacitances were low, and their changes were small when they were filled with gas under pressure. (For CO_2, the ranges were $0.718\ \text{pF} \leqslant C_{TB} \leqslant 0.751\ \text{pF}$ and $0.518\ \text{pF} \leqslant C_{IO} \leqslant 0.546\ \text{pF}$; the ranges were smaller for the other gases.) Thus, the bridge noise and its linearity for small capacitance changes were also important.

The standard deviation of each bridge reading was 0.11 aF or, fractionally, 0.2×10^{-6}. To reduce noise, each capacitance "measurement" was usually computed from the average of 20 readings of the bridge. In Ref. 7 we reported the results from measuring $C_x(0)$ during an 84-day-long interval. The data were fit to a linear function of time. We found that

$(dC_x/d\text{time})/C_x = (0.74 \pm 0.69) \times 10^{-6}\,\text{year}^{-1}$, and the deviations from the fit had a standard uncertainty of 0.17 aF. These observations show that the stability of both the bridge and the cross capacitor was satisfactory.

Our ability to test the linearity of the bridge for small increments was very limited. In one test, we used two cross capacitors under vacuum. First, four capacitance measurements (C_{1TB}, C_{2TB}, C_{1IO}, C_{2IO}) were made. Then pairs of the capacitors (such as C_{1TB} and C_{2TB}) were connected in parallel, and sums (such as $C_{1TB} + C_{2TB}$) were measured. The difference between the computed sum and the measured sum was typically 2.5 aF or, fractionally, 2.0×10^{-6}. This difference was much larger than the noise of the measurement but certainly smaller than the manufacturer's specification: "accuracy of 3 ppm." The performance tests made with helium (Section 4) also tested the capacitance bridge. Over the very limited range of capacitances (0.7181 pF $\leqslant C_{TB} \leqslant$ 0.7206 pF and 0.5185 pF $\leqslant C_{IO} \leqslant$ 0.5203 pF), the measured values of $C_x(p)/C_x(0)$ had an rms deviation of 0.14×10^{-6} from the calculated values. This test did not use fitted parameters; thus, it rigorously tested the entire measurement system.

Because $\varepsilon(p, T)$ was computed from capacitance ratios, we expected that its uncertainty would be $\sqrt{2}$ times the uncertainty of a single capacitance measurement: 4.2×10^{-6}. The tests that we have described are with this expectation. The results for helium (Section 4.1) are consistent with ratio measurements that are approximately 10 times more accurate than this.

3.4. Test Gases

All the test gases were used as purchased. Both the helium and the argon were purchased from Matheson Gas Products. The vendor specified that both gases had "99.9999% minimum purity" by volume. The vendor specified that the water content of the helium was $< 0.2 \times 10^{-6}$, by volume, and the water content of the argon was $< 1 \times 10^{-6}$, by volume. Both the nitrogen and the methane were purchased from Messer MG Industries. The vendor described both as "scientific grade" and specified their purity as "$>$99.9995% by volume." The vendor specified that the water content of the nitrogen was $< 0.9 \times 10^{-6}$, by volume, and the water content of the methane was $< 1.8 \times 10^{-6}$, by volume. The carbon dioxide was purchased from Air Products & Chemicals, Inc. The vendor described the gas as "Research Grade $>$99.995%" and specified the water content as $< 5 \times 10^{-6}$, by mole fraction.

In dielectric studies, water is a particularly obnoxious impurity because its molar polarizability is comparatively large. For water vapor near 50°C, $A_\varepsilon \approx 68\,\text{cm}^3 \cdot \text{mol}^{-1}$. This value of A_ε is 10 times larger than the

A_ε for methane and 130 times larger than the A_ε for helium. If the methane contained as much water as the vendor's specification permitted, the measured value of A_ε for methane would exceed the value for pure methane by the fraction 18×10^{-6}. Thus, the possible water content of the methane is half as important as the uncertainty of the pressure measurements (32×10^{-6} at 7 MPa). Similar remarks apply to helium, argon, and nitrogen. However, if the CO_2 contained a mole fraction 5×10^{-6} of water, its molar polarizability would be overestimated by the fraction 46×10^{-6}. For CO_2, the uncertainty of the water content is more important than the uncertainty of the pressure measurements; however, both are less important than the uncertainty of the equation of state because CO_2 was studied near its critical temperature. Precautions were taken to avoid contaminating the test gases. The cross capacitor itself was made of superinvar and sapphire. The capacitor was surrounded by an aluminum shield and supported on a superinvar plate. The pressure vessel was made of stainless steel and sealed with copper gaskets. High-vacuum construction techniques were used. Thus, threaded holes were vented and the coaxial cable within the pressure vessel was insulated with loosely fitting glass beads. The manifold leading from the cylinders suppling gas to the pressure vessel was made almost entirely of metal. A trap protected the manifold from backstreaming vacuum pump oil. No polymers were used within the pressure vessel; however, the commercially manufactured pressure controller does contain polymer valve seats, and these could not be baked. Before the controller was used, it was repeatedly flushed with each test gas.

Each measurement cycle began with the capacitor evacuated. Typically, the pressure was raised in 1-MPa steps up to 7 MPa and then lowered in 1-MPa steps. Following each pressure change, an interval of 3 to 7 h elapsed to allow the capacitor to return to thermal equilibrium. Thus, a complete cycle of 12 steps took several days. With each test gas, at least two complete measurement cycles were conducted. The data from the last cycle are reported in Table I; however, no significant differences between the last two cycles were ever detected.

4. PERFORMANCE TEST OF THE CROSS CAPACITOR

4.1. Measurements of C_x Under Helium Pressure

We tested the entire measurement system comprising the cross capacitor, the capacitance bridge, and the instruments to measure the temperature and the pressure. For this test, we measured the cross capacitance $C_x(p)$ as a function of the pressure when the capacitor was filled with

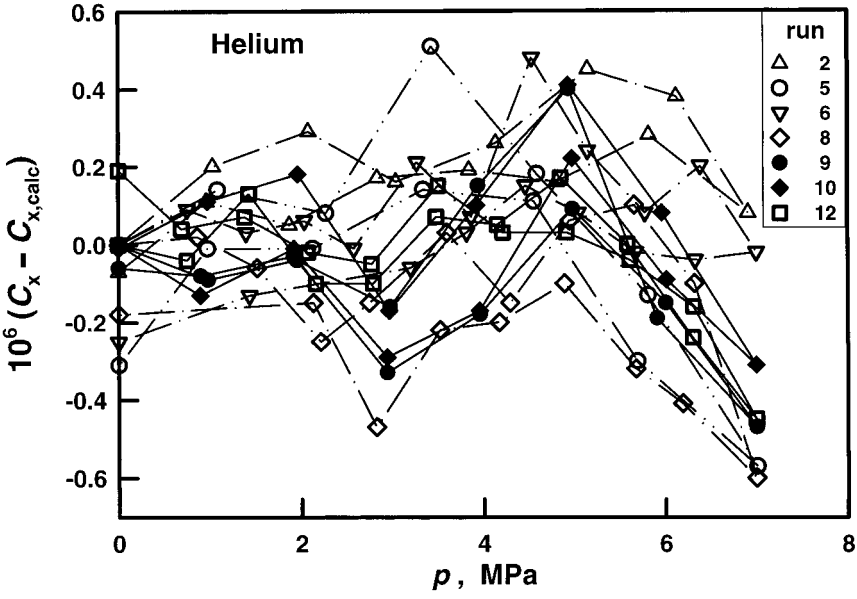

Fig. 3. Differences between calculated and measured cross capacitance as a function of pressure of helium. During each run, the pressure was increased from 0 to 7 MPa and then decreased to either 1 or 0 MPa. Incomplete runs are not plotted.

helium. (Temperature-dependent tests are reported in Ref. 7.) Figure 3 displays the fractional differences between the measured values of $C_x(p)$ and those calculated using $C_x(0)$, k_T, and the data for the properties of helium taken from the literature. The rms fractional difference is 0.27 ppm. Thus, the entire measurement system behaved as expected, almost within the reproducibility of the measurements. The measurements shown in Fig. 3 were made in seven "runs" during a 2-week-long interval. We emphasize that no parameters were fitted to the helium data in comparing the measurements with the calculations. We now describe this performance test in more detail.

At each value of the pressure where $C_x(p)$ was measured, the density and the dielectric constant were eliminated numerically from Eqs. (2), (5), and (6) to obtain predicted values of $C_x(p)$ that are denoted $C_{x,\,calc}(p)$. This procedure requires values for all of the properties of helium that appear in Eqs. (2), (5), and (6). The procedure also requires two properties of the capacitor, k_T and $C_x(0)$. We now consider the sources and uncertainties of these values.

For this test, the most important properties of helium are A_ε and B. Both A_ε and B can be calculated more accurately *ab initio* than they can

be measured. We used the *ab initio* value $A_\varepsilon = (0.517\,2539 \pm 0.000\,0010)$ $cm^3 \cdot mol^{-1}$ that was recently calculated by Pachuck and Sapirstein [12] and, independently, by Cencek et al. [13]. We used the *ab initio* value $B(50°C) = (11.703 \pm 0.025)$ $cm^3 \cdot mol^{-1}$ from Hurly and Moldover [14]. We used the values $C = (102.5 \pm 2.9)$ $cm^6 \cdot mol^{-2}$ and $D = (729 \pm 94)$ $cm^9 \cdot mol^{-3}$ from Blancett et al. [15]. Two recent calculations and an experiment are consistent with $b(50°C) = (-0.06 \pm 0.01)$ $cm^3 \cdot mol^{-1}$ [16]. White and Gugan [17] reviewed the measurements of the dielectric viral coefficients of helium and recommended the value $c = (-1.75 \pm 0.15)$ $cm^6 \cdot mol^{-2}$ for use near 298 K. To describe the sensitivity of the calculated values of $C_x(p)$ to the properties of helium, we list the fractional change in $C_{x,\,calc}(7\ MPa)$ upon increasing each property by its uncertainty: A_ε, 0.06 ppm; B, 0.24 ppm; C, 0.07 ppm; D, 0.01 ppm; b, -0.10 ppm; and c, 0.00 ppm.

As discussed in Section 2.2, the uncertainty of k_T is equivalent to 1.1×10^{-4} $cm^3 \cdot mol^{-1}$. This uncertainty contributes 0.80 ppm to the uncertainty of $C_x(7\ MPa)$, far more than all the contributions from the properties of helium. If k_T were seriously in error, the deviations in Fig. 3 would have an easily-seen linear pressure dependence.

The uncertainties of the experimental values of $C_x(p, T)$ depend upon the uncertainties of the measured capacitance, pressure, and temperature. Among these uncertainties, we expected that the uncertainty of the capacitance bridge (3 ppm) would be the most important. The deviations in Fig. 3 are much smaller than 3 ppm, showing that the ratios $C_x(p)/C_x(0)$ were more accurate than a worst-case expectation. However, the hysteresis of the deviations resulted from the pressure transducer, and by elimination of other factors, we concluded that the pressure-dependent trends in the deviations resulted from small imperfections of the capacitance bridge. The experimental values of $C_x(p)$ also depend upon the weight w used in Eq. (1) to compute the cross capacitance from its component capacitances. If w were increased by 0.01 from its optimum value 0.4476, C_x would increase by $0.22\ ppm \times p/(7\ MPa)$.

The density and dielectric virial equations are truncated expansions. Possible errors resulting from the truncation can be assessed by examining successive terms. In this work at 50°C, the highest density of helium was 2529 $mol \cdot m^{-3}$. Under these conditions, the terms $B\rho$, $C\rho^2$, and $D\rho^3$ in the pressure series [Eq. (6)] are 0.029, 0.000 66, and 0.000 012, respectively. The terms $b\rho$ and $c\rho^2$ in the molar polarizability series [Eq. (2)] are $-0.000\,22$ and 0.000 011. Both series converge rapidly, and their last retained terms change the calculated values of $C_x(7\ MPa, 50°C)$ by less than those caused by the uncertainties of k_T, A_ε, and B.

In summary, the largest systematic uncertainty $C_{x,\,calc}(p)$ comes from the uncertainty of the parameter k_T that determines the capacitor's

response to hydrostatic pressure and the largest uncertainty in the measured values of C_x comes from the capacitance bridge. The values of $|C_x - C_{x,\,calc}|$ are smaller than we expected.

4.2. Pressure Dependence of C_{TB}/C_{IO}

If the geometry of the cross capacitor and its shield were stable, the ratio C_{TB}/C_{IO} would be independent of pressure, temperature, and the dielectric constant of the gas. As Fig. 4 shows, C_{TB}/C_{IO} decreased as the pressure increased and C_{TB}/C_{IO} had hysteresis. We do not understand the origin of either behavior; however, neither behavior influenced the results for C_x.

The data for C_{TB}/C_{IO} fell into two groups. During most runs, the ratio behaved as illustrated for argon and CO_2 in the upper panel in Fig. 4. When the pressure was increased from vacuum to 7 MPa, the ratio decreased from 1.38508 by 0.00007, independent of the gas under study. Using the horizontal axis in Fig. 4, the hysteresis of the ratio was equivalent to 300 kPa or less. On occasion, notably during the interval June 26 to July 13, 2000, the ratio behaved as illustrated by the data for methane and for helium, run 10. The ratio decreased by only 0.00003 and showed hysteresis equivalent to 2 to 3 MPa. During helium run 12, the thermostat went out of control, and by the end of the measurement cycle, the bath was at 50.5°C. At the end of that run, the ratio C_{TB}/C_{IO} was 1.38505, and it did not return to its initial value (1.38508) until the temperature returned to 50°C.

The lower panel in Fig. 4 shows that the pressure dependences of C_x were similar (to within a few parts in 10^7) during helium runs 10 and 12, even though the ratio C_{TB}/C_{IO} differed by as much as 500 parts in 10^7 between the same runs.

In summary, Sections 4.1 and 4.2 demonstrate that the measured pressure dependence of C_x agreed with that calculated using Eq. (5) and the measured value of k_T. This agreement occurred in spite of the unexplained pressure dependence and hysteresis of C_{TB}/C_{IO}.

4.3. Other Tests

In Ref. 7, we described measurements of the average temperature dependence of C_x over the interval 7 to 50°C. The result was $\langle (dC_x/dT)/C_x \rangle = (5.4 \pm 0.4) \times 10^{-8}\ K^{-1}$, which is close to the negative value $-10 \times 10^{-8}\ K^{-1}$ that we calculated from the cross-capacitor design and published

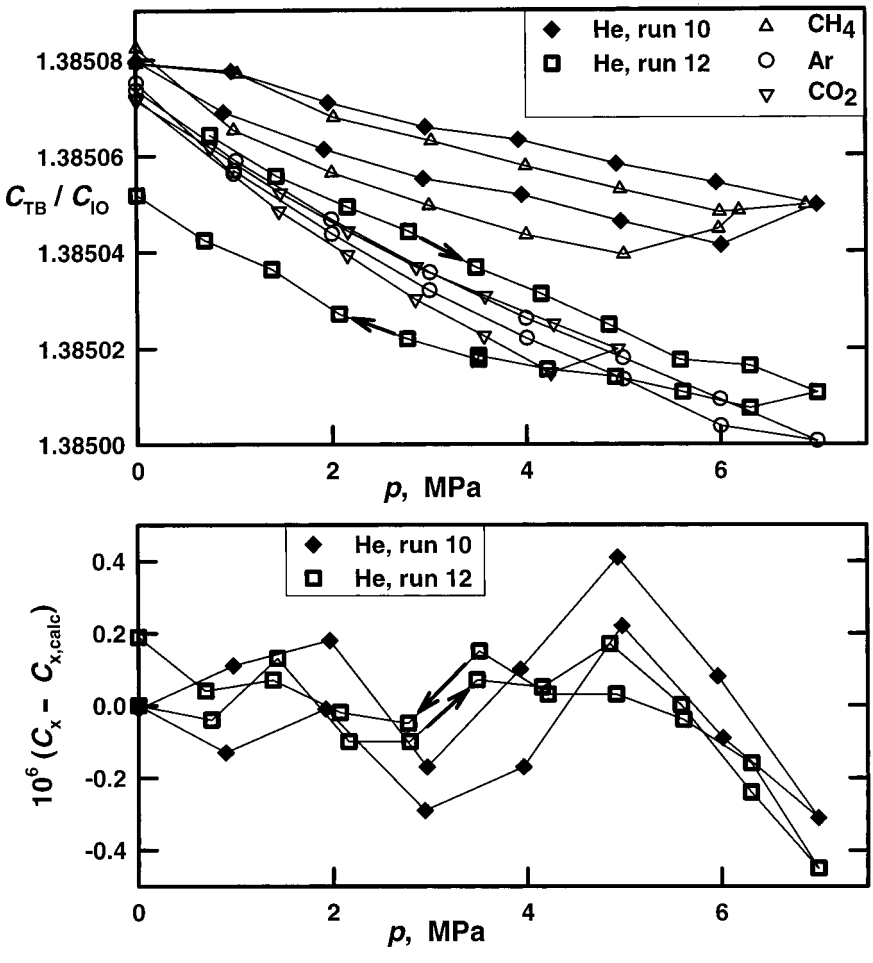

Fig. 4. Top: Measurements of the ratio C_{TB}/C_{IO} as a function of pressure. The data for methane and helium, run 10, have a weaker pressure dependence and more hysteresis than the other data. The arrows indicate the order of the data for helium, run 12. During that run, the thermostat went out of control, and at the end of the run, C_{TB}/C_{IO} did not return to its initial value. Bottom: Differences between measured and calculated values of C_x for two helium runs. The values of C_x were not affected by the different behaviors of C_{TB}/C_{IO} during the two helium runs.

data for superinvar and sapphire. These values are much smaller than the linear coefficient of thermal expansion of most metals (e.g., 1800×10^{-8} K^{-1} for typical stainless steels). Reference 7 also describes measurements of $\varepsilon(p, 7°C)$ extending up to 3 MPa. The results of these tests are entirely consistent with the behavior presented here.

5. RESULTS FOR TEST GASES

Our results for $\varepsilon(p, 50°C)$ appear in Table I. We computed ε from Eq. (5) using the value of C_x at the beginning of each measurement cycle. The negative value of $100 \times (\varepsilon - 1)$ at the end of the measurement cycle for nitrogen indicates that the final value of C_x was slightly smaller than the initial value. The tabulated pressures are the readings of the pressure transducer corrected by a calibration function (see Section 3.1) and corrected to 50°C (Section 3.2). Because the calibration function averaged over the transducer's hysteresis, the corrected pressures could be slightly negative at the end of a measurement cycle. This explains the negative pressures for the methane and helium runs in Table I.

The results in Table I can be used as reference data to test the performance of systems, such as reentrant resonators, designed to measure $\varepsilon(p, T)$. If the tests are made with helium, we recommend using calculated reference values of $\varepsilon(p, T)$, as we did in Section 4.1.

6. COMPARISON WITH RESULTS FROM THE LITERATURE

6.1. Methane

Because methane is the predominant component of natural gas, there are tabulated data for $\varepsilon(p, T)$ that can be compared with our own data. In Fig. 6, we plot $[(\varepsilon - 1)/(\varepsilon + 2)]/\rho$ for methane as a function of ρ along isotherms. In these variables, $\varepsilon(p, T)$ data spanning very wide temperature and pressure ranges collapse almost perfectly onto a single curve. The zero-pressure limit of this curve is A_ε; the slope of the curve in the limit of zero pressure is $A_\varepsilon b$. [See Eq. (2).] The experimental uncertainty of the ordinate diverges as $1/\rho = RT/\rho$ as the density approaches zero.

Figure 6 displays the low-density portion of the $\varepsilon(\rho, T)$ data tabulated by two groups: Straty and Goodwin [18] and Malbrunot et al. [19]. Both groups concentrated their efforts at higher densities and much higher pressures than in the present study (up to $28\ \text{mol} \cdot \text{dm}^{-3}$ at 34 MPa in Ref. 18 and $33\ \text{mol} \cdot \text{dm}^{-3}$ at 710 MPa in Ref. 19), and their uncertainties at the lower densities exceed our uncertainties. To prepare Fig. 6, we converted the data from Ref. 18 to the ITS-90 and we calculated the densities for *all* the data using the equation of state from Ref. 20 as implemented in Ref. 11.

Straty and Goodwin estimated that the uncertainty of their polarizabilities was $\pm 0.15\%$ at low densities and 0.1% at higher densities. These uncertainties are shown by error bars on two of their data in Fig. 6. Malbrunot et al. fitted their data; the resulting curve is plotted. The error bar attached to the low-pressure end of their curve is the uncertainty they

attributed to A_ε, $\pm 0.002\ \mathrm{cm^3 \cdot mol^{-1}}$. Although the Straty and Goodwin data are on several isotherms, their scatter in the range spanned by Fig. 6 is comparable to the uncertainty of the single isotherm of Malbrunot et al.

The present data for methane are bracketed by the curve of Malbrunot et al. and by the data of Straty and Goodwin. In the worst case (the lowest density), the uncertainty of the present data corresponds to $\pm 0.0008\ \mathrm{cm^3 \cdot mol^{-1}}$, and this is smaller than the plotted squares. We believe that A_ε (which is the zero-pressure intercept of the data in Fig. 6) is more accurately determined by the present data than by the data from the literature. In Section 6.4, we conclude that the present value of b is also consistent with, but less accurate than, the literature values for methane.

6.2. Conversion of Pressure to Density

Except for methane, we were unable to compare directly our results for $\varepsilon(p, 50°\mathrm{C})$ with previous measurements because the earlier results are not tabulated. Instead of tabulated data, several authors have published values of A_ε, $B_\varepsilon = bA_\varepsilon$, and $C_\varepsilon = cA_\varepsilon$. To obtain these coefficients from our data, we had to convert the data from $\varepsilon(p, 50°\mathrm{C})$ to $\varepsilon(\rho, 50°\mathrm{C})$ and fit the ratio $(\varepsilon - 1)/(\varepsilon + 2) = \wp\rho$ to polynomial functions of the density. Table II compares the resulting values of A_ε, b, and c with previously published values.

Ideally, we would have converted pressure to density using equations of state that were optimized for the range of the present data. Generating such equations is beyond the scope of this work. Instead, we used the wide-range equations in NIST Standard Reference Database 12, Version 5.0 [11]. For some gases, NIST12 recommends one equation of state and provides several others. We used the recommended ones, which came from the following sources: methane [20], argon [21], carbon dioxide [22], and nitrogen [23]. The conversion was done with a precision of six significant figures.

The conversion from pressure to density introduces the uncertainties of the equations of state into the determination of b and c. To estimate these uncertainties for b, we noted that our measurements of $C_x(p)$ determine A_ε and β in Eq. (7) very accurately. Equation (8) then implies that the uncertainty of b will be comparable to that of the density virial coefficient B. For argon, nitrogen, and methane, reliable values of B near 50°C from different laboratories are bracketed by ± 0.15, ± 0.2, and $\pm 0.35\ \mathrm{cm^3 \cdot mol^{-1}}$, respectively [24]. These values appear in parentheses in Table II as contributions to the uncertainty of b. These values may be too large because the equation of state is known more accurately than its components, $B\rho$, $C\rho^2$,..., and it is the equation of state itself that we used when determining b. For helium, we used the *ab initio* value of B and its

Table II. Coefficients of the Polynomial Expansion of $(\varepsilon-1)/(\varepsilon+2)$ as a function of ρ from Various Sources[a]

A_ε ($cm^3 \cdot mol^{-1}$)	b ($cm^3 \cdot mol^{-1}$)	c ($cm^6 \cdot mol^{-2}$)	T (°C)	Reference
		Methane		
6.5473 (03) (01)[b]	1.04 (01) (35)[c]	0	50	This work[d]
6.5468 (06) (01)[b]	1.12 (08) (35)[c]	−19 (18)[e]	50	This work
6.541 (03)	1.114 (49)	−41 (8)	49	Bose et al. [32]
6.551 (02)	1.10 (14)	−38 (8)	25	Malbrunot et al. [19]
		Argon		
4.14178 (11) (11)[b]	0.32 (01) (15)[c]	0	50	This work[d]
4.14133 (22) (11)[b]	0.43 (05) (15)[c]	−26 (11)[e]	50	This work
4.1397 (06)	0.174 (29)		50	Bose and Cole [30]
4.142 (02)	0.091 (05)		25	Orcutt and Cole [26]
	0.295 (22)	−18 (10)[e]	30	Huot and Bose [29]
4.146 (03)	0.191 (24)	−11 (03)	25	Vidal and Lallemand [28]
4.140 (03)			7 to 57	Goodwin et al. [2]
		Carbon dioxide		
7.34644 (47) (99)[f] (11)[b]	7.44 (07) (46)[f]	−477 (38) (150)[f]	50	This work[d]
7.350 (06)	6.90 (12)	−342 (32)	50	Bose and Cole [30]

		Nitrogen		
4.38786 (10) (11)[b]	0.40 (01) (20)[c]	0	50	This work[d]
4.38769 (23) (11)[b]	0.44 (05) (20)[c]	−11 (13)[d]	50	This work
4.3895 (05)	0.478 (23)	−31 (01)	50	Huot and Bose [27]
4.390 (02)	0.137 (46)		49	Orcutt and Cole [26]
		Helium		
0.5172539 (10)			Theory	Pachuck and Sapirstein [12]
0.51719 (07) (11)[b]	−0.29 (06) (03)[c]	0	50	This work[d]
0.5196 (02)	−0.13 (02)	−2.3 (10)	50	Huot and Bose [29]
0.5210 (02)	−0.11 (02)	−1.6 (23)	30	Kirouac and Bose [31]
0.519 (01)	−0.12 (08)		49	Orcutt and Cole [26]
0.518 (01)	−0.22 (04)			Vidal and Lallemand [28]

[a] For this work, we show the effect of the constraint $c \equiv 0$. Contributions to the uncertainty of the last two digits are shown in parentheses. The first contribution resulted from fitting routines.
[b] uncertainty from k_T.
[c] Uncertainty from B.
[d] Deviations plotted in Fig. 5.
[e] Does not include the uncertainty of the equation of state.
[f] Uncertainty from equation of state.

uncertainty, $0.025\ \mathrm{cm^3 \cdot mol^{-1}}$ [14]. Except for CO_2, the present data are at densities that are too low to determine c. Thus, we did not estimate how the conversion from pressure to density increased the uncertainty of c.

For CO_2, estimating the uncertainty of b from that of B is risky because the 50°C isotherm is near the critical temperature ($T_c \approx 31°C$) and the useful range of the virial equation is comparatively narrow. Instead, we estimated the effects of the equation-of-state uncertainties by analyzing our data using three equations of state, one [22] recommended by NIST12 and two [25] others. In Table II, we report the values of A_ε, b, and c that we obtained using the recommended equation of state, together with the standard deviation of the values obtained using all three equations of state. With the recommended equation of state, the values of A_ε, b, and c did not change when we reduced the range of the fit from 5 to 3.8 MPa. This was not true for the other two equations of state.

6.3. Fitting ε(ρ, 50°C)

When fitting $(\varepsilon - 1)/(\varepsilon + 2)$ to polynomial functions of the density, we weighted all of the values of $(\varepsilon - 1)/(\varepsilon + 2)$ equally. The fitting routine returned the values of A_ε, b, c, and their standard uncertainties which are listed in Table II. [The routine also returned $C_x(p = 0)$. These values were close to the expermental values; they are not tabulated.] In effect, the polynomial fits were averaged over the hysteresis in the data.

Table II contains two rows labeled "this work" for argon, methane, and nitrogen. For these gases, the first row came from a quadratic fit with the constraint $c \equiv 0$; the second row came from a fit without this constraint. Upon relaxing the constraint $c \equiv 0$, the values of A_ε changed by more than their tabulated uncertainties. These larger changes show the effect of truncating the dielectric virial expansion; they are better estimates of the uncertainties of A_ε than the uncertainty provided by either fit alone.

The lower plots in Fig. 5 display the deviations of our data from the coefficients in Table II. For CO_2, a cubic equation was used for the plot; for the other gases, quadratic equations were used. The deviations for methane and CO_2 are approximately twice as large as the deviations for argon, nitrogen, and helium. The deviations for methane and CO_2 are larger primarily because the equations of state of these gases are less accurate and, to a lesser degree, because $(\partial\varepsilon/\partial p)_T$ is larger for these gases.

6.4. Comparisons of A_ε, b, and c

The present work is optimized to determine A_ε. Because A_ε is a property of a single molecule, its value is independent of the equation

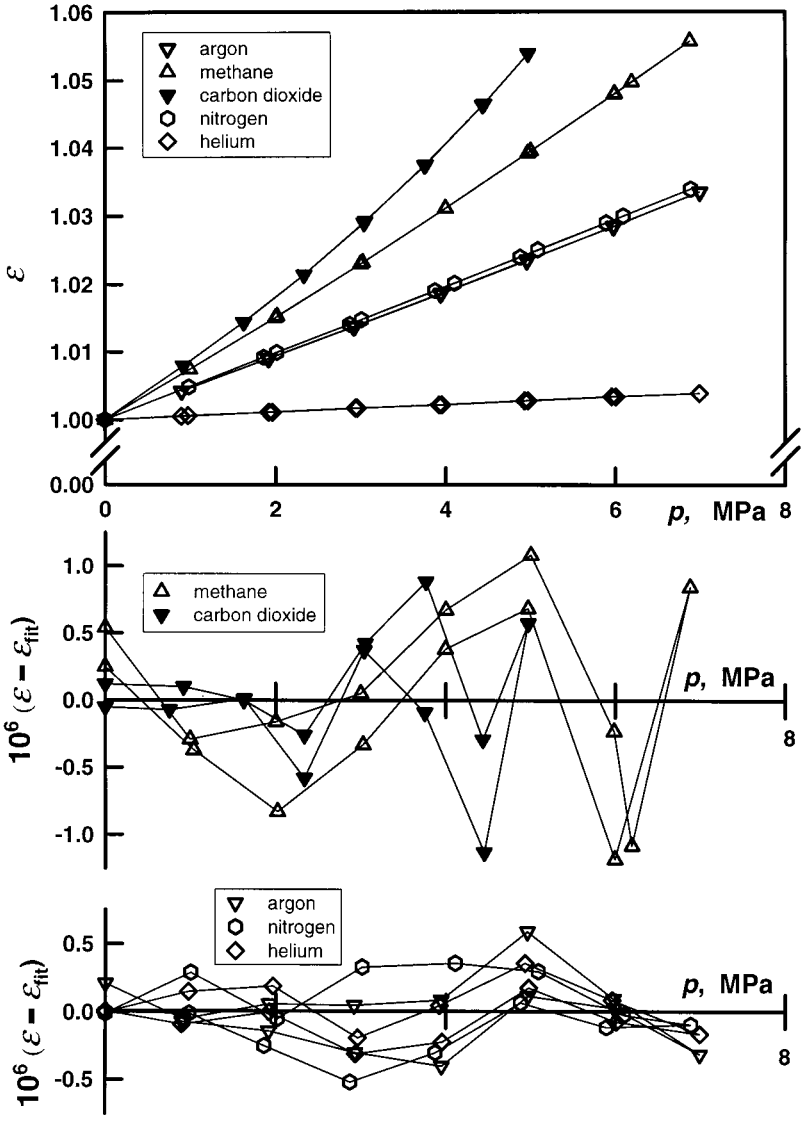

Fig. 5. Top: Dielectric constant as a function of pressure for five gases. Bottom: Differences between the measured dielectric constant and their representation by Eq. (2) using the coefficients in Table II and equations of state [11] to convert pressure to density.

of state and it is nearly independent of temperature. This permits us to compare values of A_ε determined on different isotherms. For helium, the present value of A_ε agrees with the very accurate *ab initio* value [12]. For argon, the present value of A_ε agrees with two less precise values, one reported by Orcutt and Cole [26] and a second obtained by one of us using a reentrant resonator [2]. For nitrogen, the present value of A_ε almost agrees with the value reported by Huot and Bose [27].

It is noteworthy that seven of the values of A_ε in Table II do not agree with the present values (and in the case of helium, the *ab initio* value) within the combined uncertainties. For these seven, the gases and citations are as follows: methane, Malbrunot et al. [19]; argon, Vidal and Lallemand [28] and Huot and Bose [29]; and helium, Huot and Bose [29], Bose and Cole [30], and Kirouac and Bose [31]. Measured values of A_ε could be in error if the deformations of the capacitors under pressure did not conform to those calculated from their designs. (Six of these seven values of A_ε are larger than the present values.) Alternatively, the uncertainties ascribed to the published values of A_ε could be too small. This alternative was the conclusion of Malbrunot et al. [19] when assessing the uncertainty of their own results for methane. They stated that their value of A_ε [$(6.551 \pm 0.002)\,\mathrm{cm}^3 \cdot \mathrm{mol}^{-1}$ at 298 K] agrees "within the experimental uncertainty" with the value [$(6.541 \pm 0.003)\,\mathrm{cm}^3 \cdot \mathrm{mol}^{-1}$ at 322.5 K] that Bose et al. [32] had reported much earlier.

Table II lists the literature values of $b = B_\varepsilon/A_\varepsilon$ and $c = C_\varepsilon/A_\varepsilon$, and their uncertainties, as provided by the various authors. Most of the published values of B_ε and C_ε were obtained using an expansion method. The expansion methods employ two or three nearly identical capacitors enclosed in nearly identical pressure vessels to obtain values of b and c that are, theoretically, only weakly dependent on the equation of state [33, 34]. In most cases, the reported uncertainties resulted from fitting the expansion data and they do not include explicit contributions from systematic effects such as adsorption (to which the cross capacitor is insensitive), hysteresis in pressure transducers, and unexpected pressure dependences of the capacitors (which we encountered in the ratio $C_{\mathrm{TB}}/C_{\mathrm{IO}}$).

For methane, Bose et al. [32] published values of A_ε, B_ε, and C_ε at 280, 323, and 373 K. We used these values to plot the three smooth curves labeled "Bose et al." in Fig. 6. We varied A_ε, B_ε, and C_ε within their uncertainties to obtain the error bars that are attached to the ends of these curves. (These error bars may be too small, according to Malbrunot et al.'s remark, quoted above [19].) These three curves have a small temperature dependence at low densities that the authors attributed to a real temperature dependence of B_ε [32]. In contrast, the data of Straty and Goodwin, spanning an equally wide temperature range, do not show a temperature

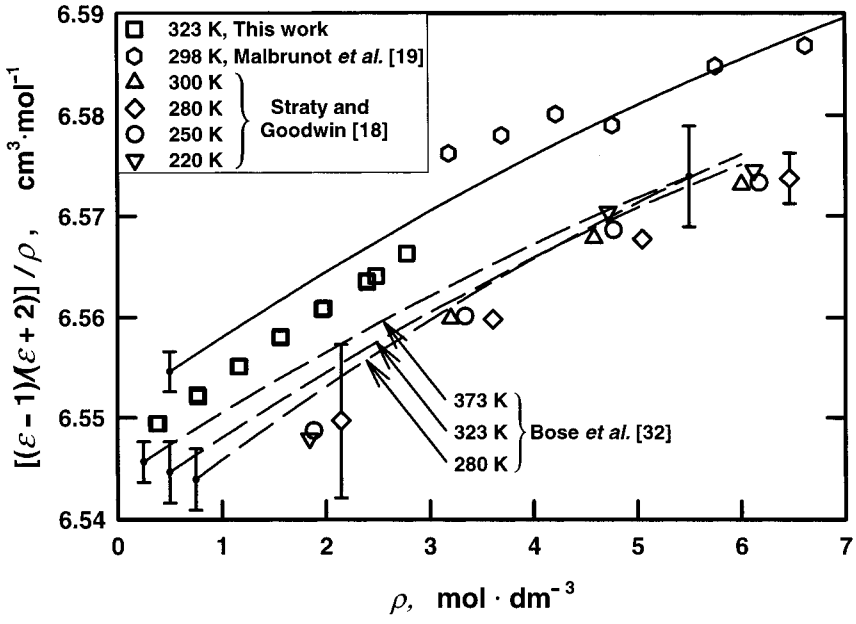

Fig. 6. Methane results from various sources. The plotted symbols were calculated using the equation of state from Ref. 20 and the $\varepsilon(p, T)$ data from this work, Straty and Goodwin [18], and Malbrunot et al. [19]. The curves represent Eq. (2) using the values of A_ε, b, and c from Bose et al. [32] and Malbrunot et al. [19].

dependence. In Fig. 6, the slope of our data is steeper than the curves representing the results of Bose et al. and Malbrunot et al. However, points plotted in Fig. 6 relied upon the equation of state. The equation of state contributes an uncertainty of approximately $0.35\ \mathrm{cm}^3 \cdot \mathrm{mol}^{-1}$ to the uncertainty of the slope and to our value of b. Considering this, our value of b is consistent with the literature for methane; however, our uncertainty is larger than the uncertainties claimed by Malbrunot et al. and by Bose et al.

For argon and nitrogen, the early values of B_ε from Orcutt and Cole [26] are inconsistent with the more recent values of Huot and Bose [27, 29]. The latter authors noted that their data extended to higher pressures (40 vs 10 MPa) and argued that "as Orcutt and Cole did not get a significant contribution of the C_ε term, there may be a hidden contribution from C_ε in their B_ε value." For argon and nitrogen, our data extend to 7 MPa and lead to values of b that are consistent with the later values, whether or not we fit for c.

Our data for methane, argon, and nitrogen can barely determine the sign of c because of the low densities that we used. (Table II) This is consistent

with the very small deviations that we obtained when fitting these data with the constraint $c \equiv 0$. (See the lower panel in Fig. 5.) The data of Vidal and Lallemand [28] for argon and nitrogen extend to 1200 MPa, a pressure 170 times higher than we attained. Thus, they determined c with some precision even though their uncertainties were dominated by the imprecision of the density, which was 0.1% at pressures below 100 MPa and 0.3% above 100 MPa. Huot and Bose used the expansion method to determine b and c for argon [29] and nitrogen [27].

For CO_2, our values of A_ε, b, and c agree with those of Bose and Cole [30]. Most likely, our value of A_ε is the more accurate. Bose and Cole claim smaller uncertainties for their values for b and c than we do. If they had discussed the uncertainties from the equation of state and adsorption, their claim would have been stronger [34].

ACKNOWLEDGMENTS

We thank Dr. Albert Migliori of Los Alamos National Laboratory for measuring the elastic constants of the superinvar samples. Dr. Jean Hamelin built the cross capacitor that was used in this research.

REFERENCES

1. M. Jaeschke, P. Schley, and R. Janssen van Rosmalen, Paper presented at the 14th Symposium on Thermophysical Properties, Boulder, CO, June 25–30, 2000.
2. A. R. H. Goodwin, J. B. Mehl, and M. R. Moldover, *Rev. Sci. Instrum.* **67**:4294 (1996).
3. J. O. Hamelin, J. B. Mehl, and M. R. Moldover, *Int. J. Thermophys.* **19**:1359 (1998).
4. A. M. Thompson and D. G. Lampard, *Nature (London)* **177**:888 (1956).
5. D. B. Lampard, *Proc. IEE Monogr. H*, *216M* **104C**:271 (1957).
6. D. Makow and J. B. Campbell, *Metrologia* **8**:148 (1972); J. B. Campbell and D. Makow, *J. Comput. Phys.* **12**:137 (1973).
7. T. J. Buckley, J. Hamelin, and M. R. Moldover, *Rev. Sci. Instrum.* **71**:2914 (2000).
8. J. Q. Shields, *IEEE Trans. Instrum. Meas.* **IM-27**:464 (1978).
9. W. Chr. Heerens, B. Cuperus, and R. Hommes, *Delft Progress Rep.* **4**:67 (1979).
10. A. Migliori and J. L. Sarro, *Resonant Ultrasound Spectroscopy* (John Wiley, New York, 1997).
11. E. W. Lemmon, A. W. Peskin, M. O. McLinden, and D. G. Friend, NIST Standard Reference Database 12, Version 5.0 (U.S. Department of Commerce).
12. K. Pachuck and J. Sapirstein, *Phys. Rev.* **A63**:012504 (2000).
13. W. Cencek, K. Szalewicz, and B. Jeziorski, submitted for publication.
14. J. J. Hurly and M. R. Moldover, *J. Res. Natl. Inst. Stands. Tech.* **105**:667 (2000).
15. A. L. Blancett, K. R. Hall, and F. B. Canfield, *Physica* **47**:75 (1970).
16. H. Koch, C. Hättig, H. Larsen, J. Olsen, P. Jørgensen, B. Fernández, and A. Rizzo, *J. Chem. Phys.* **111**:10108 (1999).
17. M. P. White and D. Gugan, *Metrologia* **29**:37 (1992).
18. G. C. Straty and R. D. Goodwin, *Cryogenics* **13**:712 (1973).

19. P. Malbrunot, J. Vermesse, D. Vidal, T. K. Bose, A. Hourri, and J. M. St-Arnaud, *Fluid Phase Equil.* **96**:173 (1994).
20. U. Setzmann and W. Wagner, *J. Phys. Chem. Ref. Data* **20**:1061 (1991).
21. Ch. Tegeler, R. Span, and W. Wagner, *J. Phys. Chem. Ref. Data* **28**:779 (1999).
22. R. Span and W. Wagner, *J. Phys. Chem. Ref. Data* **25**:1509 (1996).
23. R. Span, E. W. Lemmon, R. T. Jacobsen, and W. Wagner, *J. Phys. Chem. Ref. Data* (in press. See also *Int. J. Thermophys.* **14**:1121 (1998).
24. J. P. M. Trusler, W. A. Wakeham, and M. P. Zarari, *Mol. Phys.* **90**:695 (1997).
25. J. F. Ely, J. W. Magee, and W. M. Haynes, *Thermophysical Properties for Special High CO_2 Content Mixtures*, Research Report RR-110 (Gas Processors Association, Tulsa, OK, 1987). (This report contains two equations of state).
26. R. H. Orcutt and R. H. Cole, *J. Chem. Phys.* **46**:697 (1967).
27. J. Huot and T. K. Bose, *J. Chem. Phys.* **94**:3849 (1991).
28. D. Vidal and M. Lallemand, *J. Chem. Phys.* **64**:4293 (1976).
29. J. Huot and T. K. Bose, *J. Chem. Phys.* **95**:2683 (1991).
30. T. K. Bose and R. H. Cole, *J. Chem. Phys.* **52**:140 (1970).
31. S. Kirouac and T. K. Bose, *J. Chem. Phys.* **64**:1580 (1976).
32. T. K. Bose, J. S. Sochanski, and R. H. Cole, *J. Chem. Phys.* **57**:3592 (1972).
33. A. D. Buckingham, R. H. Cole, and H. Sutter, *J. Chem. Phys.* **52**:5960 (1970).
34. H. Sutter and R. H. Cole, *J. Chem. Phys.* **52**:132 (1970).